

# Monte Carlo simulations of infinitely dilute solutions of amphiphilic diblock star copolymers

Ronan Connolly<sup>†</sup>

*Theory and Computation Group, Department of Chemistry, University College Dublin, Belfield, Dublin 4, Ireland*

Edward G. Timoshenko\*

*Theory and Computation Group, Centre for Synthesis and Chemical Biology, Conway Institute of Biomolecular and Biomedical Research, Department of Chemistry, University College Dublin, Belfield, Dublin 4, Ireland*

Yuri A. Kuznetsov<sup>‡</sup>

*Centre for High Performance Computing Applications, University College Dublin, Belfield, Dublin 4, Ireland*  
(September 29, 2018)

Single-chain Monte Carlo simulations of amphiphilic diblock star copolymers were carried out in continuous space using implicit solvents. Two distinct architectures were studied: stars with the hydrophobic blocks attached to the core, and stars with the polar blocks attached to the core, with all arms being of equal length. The ratio of the lengths of the hydrophobic block to the length of the polar block was varied from 0 to 1. Stars with 3, 6, 9 or 12 arms, each of length 10, 15, 25, 50, 75 and 100 Kuhn segments were analysed. Four distinct types of conformations were observed for these systems. These, apart from studying the snapshots from the simulations, have been quantitatively characterised in terms of the mean-squared radii of gyration, mean-squared distances of monomers from the centre-of-mass, asphericity indices, static scattering form factors in the Kratky representation as well as the intra-chain monomer-monomer radial distribution functions.

## I. INTRODUCTION

Due to recent advances in ‘living’ polymer synthesis, by combining various living polymerisation techniques such as anionic, cationic, ring-opening and very recently, ‘pseudo-living’ controlled radical polymerisations such as atom transfer radical polymerisations, it is now possible to synthesise quite monodisperse star-branched polymers (i.e., a polymer with a single branch point, the core, with all the branches, arms, of equal length), with a good degree of control over the length and composition of the arms as well as the number of them<sup>1–5</sup>. Star-branched diblock copolymers, where each arm consists of an identical diblock copolymer (as opposed to, for instance, heteroarm or miktoarm star copolymers, where the arms themselves are of different composition<sup>6–9</sup>) have been synthesised recently with increased success<sup>10–24</sup>.

Of late there has been some interest in the potential use of amphiphilic star copolymers<sup>15–24</sup> (where one type of monomer is hydrophobic, H, and the other type is hydrophilic or polar, P) as possible drug delivery vehicles. Star polymers have been shown to have smaller hydrodynamic radii than linear polymers<sup>16,25</sup>, which could be important in avoiding uptake by the reticuloendothelial system (RES)<sup>26</sup>, as well as having a lower crystallinity which is of importance in drug carrier design<sup>25</sup>. It has also been suggested that star copolymers could be designed which would form only unimolecular micelles in aqueous solution<sup>20,21,24</sup>. These systems would have advantages as drug delivery vehicles over conventional multimolecular copolymer micelles. Linear diblock copolymers have been found to form multimolecular micelles above the critical micellar concentrations (CMC)<sup>27–31</sup>. These systems have been touted as potential drug delivery vehicles, since they are able to encapsulate hydrophobic drugs. They can also be designed to avoid uptake by the RES<sup>23,29–31</sup>, since the polar blocks increase the ‘stealth’ characteristics of the micelles. These systems, however, are thermodynamically unstable below their CMC, and although polymeric micelles have been found to be more thermodynamically stable than the simpler surfactant micelles<sup>28,29</sup>, and they may be quite kinetically stable, suggesting that they may be able to temporarily withstand the large dilutions involved in drug delivery<sup>27,29</sup>, these systems are still quite mobile, and drug molecules may still be able to pass between the micelle

---

<sup>†</sup>E-mail: Ronan.Connolly@ucd.ie

\*Author to whom correspondence should be addressed. Internet: <http://darkstar.ucd.ie>; E-mail: Edward.Timoshenko@ucd.ie

<sup>‡</sup>E-mail: yuri@ucd.ie

and the solution<sup>26,32,33</sup>. It has been suggested that the thermodynamic instability of polymeric micelles could be overcome by constructing branched polymers, where the amphiphilic chains are covalently bound together<sup>26,32,33</sup>.

There appears to have been some success in creating these unimolecular micelles out of highly branched systems, such as dendrimers<sup>34,35</sup>, graft copolymers<sup>36,37</sup> and various other branched topologies<sup>24,26,32,33,38</sup>, however the question of whether the single branch point of star copolymers is sufficient to form unimolecular micelles, or whether they would form multimolecular micelles, appears to be one of some debate at the moment, with experimental evidence for both arguments. Regardless, it seems that some star copolymers are indeed capable of forming purely unimolecular micelles, although others form either a mixture of unimolecular micelles and multimolecular micelles<sup>20,24</sup>, or purely multimolecular micelles<sup>21,23,22</sup>.

For instance, Miller *et al* synthesised different amphiphilic star diblocks<sup>20</sup>. Using light scattering, they found that  $f = 6$  armed INNER-H and OUTER-H stars both are capable of unimolecular micelle formation, although one of the systems also showed some limited aggregation. If chloroform is chosen, which is a good solvent for their ‘H’ monomers, and a poor solvent for their ‘P’ monomers, it appears that an INNER-solvophobic  $f = 6$  star, with  $N_{\text{solvophobic}}/N \approx 0.13$  formed unimolecular micelles, with no evidence of higher molecular weight aggregates. On the other hand, an OUTER-solvophobic  $f = 6$  star, with  $N_{\text{solvophobic}}/N \approx 0.32$  did show some evidence of aggregation, although predominantly unimolecular micelles were formed.

Gnanou *et al* synthesised two INNER-H,  $f = 6$  star diblocks<sup>24</sup>. Analysis using size exclusion chromatography suggested that the stars with  $N_H/N=0.03$  formed unimolecular micelles in water. The stars with  $N_H/N=0.1$  also formed unimolecular micelles, however aggregates of several stars were also detected. Interestingly, when they changed the solvent to tetrahydrofuran (THF) (of opposite solvent quality for both monomer types), in effect changing the stars to OUTER-solvophobic topology, unimolecular micelles were still observed for the  $N_{\text{solvophobic}}/N=0.9$  star (i.e., the  $N_H/N=0.1$  star). Of course, aggregation was more dominant than in water, however a significant proportion of the conformations were suggested to be unimolecular in nature. In contrast, the  $N_{\text{solvophobic}}/N=0.97$  star (i.e., the  $N_H/N=0.03$  star) showed little tendency for unimolecular micelle formation, favouring intermolecular association.

Several groups were unable to detect unimolecular micelle formation for their synthesised amphiphilic star diblocks, instead detecting quite distinct CMC<sup>21–23</sup>. However these studies all involved  $f = 3$  or 4 armed stars, and it is possible that more arms are indeed necessary for unimolecular micelle formation, as suggested earlier.

Uhrich’s group have synthesised novel amphiphilic polymer systems, which have some similarities with  $f = 3$  star diblocks<sup>26,32</sup>. They find that these polymers appear to form unimolecular micelles exclusively in aqueous solution. Although their polymers contain only  $f = 3$  polar, poly(ethylene glycol), arms, they suggest that these arms are not fully extended, but instead wrap around the hydrophobic core, presumably offering enough ‘shielding’ to prevent intermolecular aggregation.

It seems likely that the CMC is at least significantly reduced, when present, for star diblock copolymers in comparison to linear diblock copolymers, since several of the diblocks are already covalently joined through the core monomer. There is also reason to suggest that these systems even have micellar behaviour (potentially allowing encapsulation) below their CMC<sup>22</sup>.

The single-chain behaviour of these systems seems particularly important as it serves as a prerequisite for trying to understand the effects of higher concentrations. Computer simulations have been really successful in investigating single linear chains, but there does not appear to be many computational studies of isolated amphiphilic star diblock copolymers. Aside from a previous work involving two of the coauthors of the current paper<sup>39</sup>, the only other appropriate simulational study we could find was a Monte Carlo study by Nelson *et al*<sup>40</sup>. This work had some limitations which we have previously discussed<sup>39</sup>, in particular, the fact that it was performed using a lattice. As we have previously mentioned<sup>39</sup>, lattice simulations can be problematic for branched systems. We believe that for them the additional computational expense required to run Monte Carlo simulations in continuous space is well justified and, in fact, quite important.

In our previous study of star copolymers<sup>39</sup>, we only briefly discussed the effect of varying the hydrophobic:polar (H:P) composition of the arms, with the bulk of the study being dedicated to the 50:50 cases. In reality, however, there appears to be quite a range of H:P ratios synthesised<sup>15–24</sup>. Control of the H:P ratio is particularly significant with regard to drug delivery applications. Low values of H:P seem to increase the stealth characteristics in evading uptake by the RES<sup>30,31</sup>, as well as being more likely to result in the formation of unimolecular micelles<sup>24</sup>. On the other hand, high values of H:P tend to increase the drug encapsulation ability of micelles<sup>27</sup>, while reducing the drug release rate<sup>30</sup>, as well as reducing the CMC of those systems which form multimolecular micelles<sup>27</sup>. Hence we wish to address this issue in more detail here.

Moreover, we have previously seen in Ref. 39 that an additional metastable state with compacted H subglobules at the ends of outstretched P arms occurs for the OUTER-H star copolymers. Here we would like to investigate whether this state could indeed become thermodynamically stable for some range of compositions as conjectured, as well as to look at the phase diagram of such stars more generally. Also, we would be interested to study several useful observables of star copolymers, most of which are experimentally measurable, such as the asphericity characteristics,

static structure factors (SSF), and intra-chain monomer-monomer radial distribution functions (RDF), which have been recently investigated by us for the homopolymer stars and dendrimers in the good solvent<sup>41,42</sup>.

## II. MODEL AND NOTATIONS

The current coarse-grained star copolymer model is based on the following Hamiltonian (energy functional)<sup>39,41,42</sup> in terms of the monomer coordinates,  $\mathbf{X}_i$ :

$$\frac{H}{k_B T} = \frac{1}{2\ell^2} \sum_{i \sim j} \kappa_{ij} (\mathbf{X}_i - \mathbf{X}_j)^2 + \frac{1}{2} \sum_{ij, i \neq j} U_{ij}^{(lj)} (|\mathbf{X}_i - \mathbf{X}_j|). \quad (1)$$

Here the first term represents the connectivity of the star with harmonic springs of strength  $\kappa_{ij}$  introduced between any unique pair of connected monomers (which is denoted by  $i \sim j$ ). It should be noted that we define a ‘monomer’ in relation to the Kuhn length of the polymer, and hence more detailed bonded terms are not essential here. The second term represents pair-wise non-bonded, viz., van der Waals, interactions between monomers. We shall adopt the Lennard-Jones form of the potential,

$$U_{ij}^{(lj)}(r) = \begin{cases} +\infty, & r < d^{(0)} \\ U_{ij}^{(0)} \left( \left( \frac{d^{(0)}}{r} \right)^{12} - \left( \frac{d^{(0)}}{r} \right)^6 \right), & r > d^{(0)} \end{cases}, \quad U_{ij}^{(0)} = \frac{1}{2} \left( U_i^{(0)} + U_j^{(0)} \right). \quad (2)$$

with a hard core part and the monomer diameter  $d^{(0)}$  (equal for H and P monomers in this work), which will be chosen to coincide with  $\ell$  here, where  $U_i^{(0)}$  is the dimensionless strength of the Lennard-Jones interaction acting upon monomer  $i$ .

In amphiphilic copolymers, there are two types of monomers, hydrophobic (H) and polar (P). We model the behaviour of these two types in aqueous solution with the following method incorporating the effect of the solvent into ‘effective’ monomer-monomer interactions. We define the strength of the interactions between two hydrophobic beads as  $U_{HH}^{(0)} = 5 k_B T$  here. The strength of the interactions between two polar beads is defined as  $U_{PP}^{(0)} = 0$ . We take the strength of the interactions between a hydrophobic bead and a polar bead as being the arithmetic mean of the two possible interactions, i.e.,  $U_{HP}^{(0)} = 2.5 k_B T$ . This implicit solvent model and particular choice of parameters, while physically simple, are somewhat non-trivial to derive, but they have been previously well rationalised<sup>39,43</sup>.

Strictly speaking, this model is generic in the description of the solvent, and so we could think of the monomers as solvophobic and solvophilic, but since much of the work on star diblock copolymers is interested in aqueous solution and in order to allow easy comparison with our earlier study of these systems<sup>39</sup>, it is convenient to use the hydrophobic/polar notation.

We will also use the other notations from our earlier study where appropriate: Each star consists of  $f$  arms, or functionalities, attached to a single core monomer. The total number of monomers is defined as  $N + 1$ , resulting in  $N/f$  monomers in each arm, assuming that all arms are of the same length. For diblock stars, consisting of a block of H beads and a block of P beads, we will refer to the situation where the H-block is attached to the core monomer and the P-block is on the outside as ‘INNER-H’, as in our previous study<sup>39</sup>. We will refer to the reverse situation, where the P-block is attached to the core monomer and the H-block is on the outside as ‘OUTER-H’. In both cases, for simplicity, we assume that the core monomer has the properties (i.e., H or P) of the monomers to which it is attached. The composition of the arms will be denoted by the parameter,  $N_H/N$  or  $N_P/N$ , where  $N_H$  is the number of hydrophobic beads and  $N_P$  is the number of polar beads.

Now let us introduce the main observables of interest. The mean-squared (MS) radius of gyration and the MS distance of monomer  $i$  from the centre of mass, are defined respectively as,

$$\langle R_g^2 \rangle = \frac{1}{2N^2} \sum_{ij, i \neq j} \left\langle (\mathbf{X}_i - \mathbf{X}_j)^2 \right\rangle, \quad \langle R_i^2 \rangle = \left\langle \left( \mathbf{X}_i - \frac{1}{N} \sum_j \mathbf{X}_j \right)^2 \right\rangle. \quad (3)$$

The asphericity and ellipsoid indices,  $A_3$  and  $S_3$  respectively, are defined as in Ref. 42, such that

$$0 \text{ (sphere)} \leq \mathcal{A}_3 \leq 1 \text{ (collinear)}, \quad -\frac{1}{4} \text{ (oblate)} \leq \mathcal{S}_3 \leq 2 \text{ (prolate)}. \quad (4)$$

The dimensionless specific heat capacity is related to the energy variance,

$$\frac{c_V}{k_B} = \frac{\langle(\Delta E)^2\rangle}{N(k_B T)^2}. \quad (5)$$

The intra-chain monomer–monomer radial distribution function (RDF) of a pair of monomers  $i$  and  $j$  is defined as,

$$g_{ij}^{(2)}(\mathbf{r}) \equiv \left\langle \delta(\mathbf{X}_i - \mathbf{X}_j - \mathbf{r}) \right\rangle = \frac{1}{4\pi r^2} \left\langle \delta(|\mathbf{X}_i - \mathbf{X}_j| - r) \right\rangle. \quad (6)$$

as in Ref. 42. The function is normalised to unity via:  $\int d^3\mathbf{r} g_{ij}^{(2)}(\mathbf{r}) = 1$ . The static structure factor (SSF), is introduced as follows:

$$S(q) = \frac{1}{N} \sum_{ij} \tilde{g}^{(2)}(|\mathbf{q}|), \quad \tilde{g}^{(2)}(\mathbf{q}) = \langle \exp(i\mathbf{q}(\mathbf{X}_i - \mathbf{X}_j)) \rangle = \frac{1}{2\pi^2} \int_0^\infty r^2 dr \frac{\sin(qr)}{qr} g_{ij}^{(2)}(r), \quad (7)$$

where tilde indicates the 3D Fourier transform, and the wave number is  $q = 4\pi \sin(\frac{\theta}{2})/\lambda$ . Partial SSFs are calculated using a similar definition, except that summation only occurs over the relevant monomers.

### III. SIMULATION TECHNIQUES

We use the Monte Carlo (MC) technique with the standard Metropolis algorithm<sup>44,45</sup> and local monomer moves based upon the implementation described by us in Refs. 39, 41, 42 and references described therein. A Monte Carlo sweep (MCS) is defined as  $N$  attempted MC steps. Initial conformations of stars were taken as globules obtained from simulations of the equivalent homopolymers in poor solvent. This was done in order to reduce computational expense and avoid possible metastable states which were observed in a previous study<sup>39</sup>, as it takes longer for two H beads to meet than for two P beads to separate. These conformations were however then subjected to extensive equilibration for a required time before any simulation was commenced.

To ensure good equilibration, the behaviour of global observables such as the energy and radius of gyration were monitored. After reaching equilibrium, a large number of statistical measurements were performed. To ensure statistical independence of sampling, each consecutive measurement was separated by a large number of MCS. The number of MCS required between each measurement, was calculated by ensuring that the ‘statistical inefficiency’,  $s$ , of relevant observables tended towards 1, as described in Ref. 45. The mean value and error of sampling of an observable  $A$  are then given by the arithmetic mean  $\langle A \rangle = (1/Q) \sum_\gamma^Q A_\gamma$  and by  $\pm \sqrt{(\Delta A)^2/Q}$  respectively, where  $Q$  is the number of statistically independent measurements<sup>46</sup>. As in our previous works<sup>39,42,41</sup>, energies will be reported in units of  $k_B T$  and distances will be reported in units of  $\ell$ .

### IV. RESULTS FROM MONTE CARLO SIMULATIONS

We have studied diblock star copolymers with  $f = 3, 6, 9$  and 12 arms, each of length  $N/f = 10, 15, 25, 50, 75, 100$  monomers. The relative ratio of the length of the P-block to the total arm length was varied from  $N_P/N=0$  to 1. Obviously, since the arms were of finite length, only certain discrete values of this ratio were permitted. The two distinct INNER–H and OUTER–H topologies described in Section II were investigated.

#### A. Possible conformations and phase diagram

Four distinct types of conformations were observed for these systems, labeled A, B, C and D in Fig. 1. Types A and B correspond to those previously observed in Ref. 39. Namely, for INNER–H stars, the H beads cluster together to form a globule, while the monomers in the P-blocks behave as coils, albeit attached to the globule, resulting in the usual micellar conformations (type A). For most OUTER–H stars a micellar type of conformation is also observed, with the H beads forming a globule and the P-blocks having coil-like behaviour, although in this case, due to connectivity constraints, the P-blocks are all attached to the polar core monomer located outside the H globule, as well as to the H globule itself. Such a conformation (type B) can hence be described as a micelle with daisy-like loops, or loopy micelle in brief. It can be seen that the extra attachment of the P-blocks necessary for type B is entropically unfavourable, although energetically favourable as it permits the H beads to form a compact globule, resulting in an overall lowering of the Helmholtz free energy. However, if the number of H beads is decreased, corresponding to larger values of  $N_P/N$ ,

then this lowering in energy is reduced and may not be enough to counteract the loss in entropy required for the H beads at the ends of each P-block to meet. Hence for large values of  $N_P/N$  another type of conformation (type D) is observed, where the H-beads at the end of each arm form separate globules. Here, however, these globules do not coalesce, and so the observed conformations are akin to those of star homopolymers in good solvent, although with  $f$  clusters of H beads at the ends of the arms. A typical snapshot with this type of conformation is illustrated in Fig. 2b. Although such a shape corresponded to a metastable conformations for compositions considered in Ref. 39, these conformations, in the area of the phase diagram designated as D, correspond to the true equilibrium structures. These never change during the equilibrium simulation no matter how long and, importantly, do not depend on the initial conformation or the pathway leading to the part D of the phase diagram, reaffirming that the state is indeed an equilibrium one.

For slightly smaller values of  $N_P/N$ , an intermediate regime is observed, where some of these globular clusters can coalesce, but not all of them together. We refer to these types of conformations as type C. In this area of the phase diagram, C, states with such partial clustering have a lower free energy than any of the states B or D, and hence the area C also corresponds to equilibrium structures, related to different ways of clustering in its different parts, and not merely local free energy minima. However, interestingly, some of these globular clusters can enter and leave the larger globular subglobules throughout the course of the simulation, indicating that the barriers between such distinct minima are fairly low. For instance, a typical snapshot of type C is illustrated in Fig. 2a. Although there are three clusters of H beads (black) in this snapshot, the actual number of clusters varied from three to five in the course of the simulation. An analysis of the energy suggests that any energy barriers between these different structures are easily traversed by the thermal fluctuations present in the simulation, although the entropy difference between such states is hard to quantify from the Monte Carlo data. The resulting cluster size distribution is a fairly broad one, as opposed to the fairly narrow aggregation size distributions seen previously for the ‘mesoglobules’, which represent multimolecular self-assemblies of linear heteropolymers of certain sequences in narrow strips of the phase diagram<sup>43</sup>.

A comparison of the heat capacity values presented in Fig. 3 for stars with  $f = 6$  arms of length  $N/f = 50$  beads reveals its relatively high values for the systems which adopt conformations of type C, i.e., those where  $N_H/N = 0.1, 0.12$  and  $0.14$ . This is indicative of greater fluctuations in energy associated with several differently clustered conformations with low enough energy barriers between the corresponding energy minima that are thermally accessible to the system. Increasing the length of the arms reduces the entropic loss required for conformations of type B, and so the range of values of  $N_P/N$  with conformations type B is increased. Changing the number of arms with a fixed arm length,  $N/f$ , did not seem to have any significant effect on the phase diagram, although stars with more than  $f = 12$  arms were not studied in this work. Therefore, we could extrapolate the phase boundaries between B, C and D regions using the data available for stars with different number of arms  $f = 3, 6, 9$  and  $12$ .

With these four types of conformations in mind, it is possible to explain the different values of MS radii of gyration,  $\langle R_g^2 \rangle$ , which can be used as an indicator of the size of the polymer plotted in Fig. 4 vs  $N_H/N$  for INNER-H and OUTER-H stars. In Fig. 4, we only discuss  $\langle R_g^2 \rangle$  for stars with  $f = 6$  arms of length  $N/f = 50$  beads, however the other systems studied were qualitatively similar. For INNER-H stars there is a relatively uniform decrease in  $\langle R_g^2 \rangle$  with increasing  $N_H/N$ , since the compact globular component of the micelles increasingly dominates the size as the relative fraction of the H beads is increased. A similar behaviour is observed for the OUTER-H stars with  $N_H/N > 0.14$ , corresponding to conformations of type B (loopy micelles) for the same reason. Clearly, it can be seen that the  $\langle R_g^2 \rangle$  values are considerably smaller for the OUTER-H stars, since the size of type B conformations is more compact due to the additional tethering of the P-blocks to the core monomer. However, for stars with  $N_H/N < 0.1$ , the OUTER-H stars in fact have higher  $\langle R_g^2 \rangle$  values than their corresponding INNER-H stars. This results from the fact that the type D conformations observed for these stars are less compact than the type A conformations, since the H beads form several clusters at the end of each outstretched arms (See Fig. 2b), instead of the single H bead globule observed for type A stars (See Fig. 1). As mentioned before, the OUTER-H stars with  $N_H/N = 0.1, 0.12$  and  $0.14$  have conformations of type C, an area where a rapid fall of the  $\langle R_g^2 \rangle$  occurs. Obviously, the stars with  $N_H/N = 0$  and  $1$  correspond to the homopolymers in good and poor solvents respectively, and hence are identical in size for ‘INNER-H’ and ‘OUTER-H’.

In order to obtain a more detailed understanding of the various types of conformations which occur for OUTER-H stars, it may be helpful to compare the MS distances plots of each bead,  $i$ , from their centre-of-mass for various values of  $N_P/N$ , shown in Fig. 5. Fig. 17 in Ref. 39 illustrates these plots for the INNER-H case, and while Fig. 18 in Ref. 39 illustrates the OUTER-H case, the plots for values of  $N_P/N > 0.8$  are not reported there. For the stars discussed here it is those values of  $N_P/N > 0.8$  which correspond to types C and D, so it is useful to explicitly include the plots for the region  $N_P/N = 0.8 - 1.0$ . The plots discussed here are again those corresponding to stars with  $f = 6$  arms, each of length  $N/f = 50$  beads. For the stars with  $N_P/N < 0.86$ , corresponding to type B (lower curves in the middle of the Fig.), the beads have a maximum value for the bead in the middle of the P-block, since the other ends are attached to either the H-globule or the core bead, as has been discussed previously in Ref. 39. The MS distances

of the H beads from the centre of mass are fairly constant and small, as is characteristic of the globules, whereas those of the P blocks are much larger and have a distorted bell shape. The stars with  $N_P/N > 0.9$  adopt conformations of type D (upper curves in the middle of the Fig.). These stars are only tethered at the core bead, hence the MS distances from the centre-of-mass, which in this case correspond to distances near the core bead, increase along the arm, until a plateau is reached for the H beads, as these are all in a subglobule and hence close to each other spatially. Intermediate values of  $N_P/N$  correspond to conformations of type C. As was already mentioned stars of this type have conformations with variable degrees of clustering. Stars of type C, which on average have larger numbers of H clusters tend to be more similar to type D than type B, e.g.,  $N_P/N = 0.9$ , while those which on average have smaller numbers of H clusters, tend to be more similar to type B than type D, e.g.,  $N_P/N = 0.86$  and  $0.88$ .

## B. Asphericity characteristics

Increasing the number of arms in homopolymer stars is known to cause more spherical conformations<sup>42,47</sup>. This also occurs for the copolymer stars discussed here, however there does not appear to be any other effect of increasing the number of arms in the range studied here, so we will limit our discussion here to the case of  $f = 6$  arms. The following discussion can also be applied to the cases of  $f = 3, 9$  or  $12$  arms, except that the absolute values of  $A_3$  and  $S_3$  decrease with increasing numbers of arms.

In Figs. 6 and 7 the asphericity and ellipsoid indices respectively of both INNER-H and OUTER-H stars with  $f = 6$  arms each of length  $N/f = 50$  beads are plotted against the H composition,  $N_H/N$ . It can be seen that OUTER-H stars of type B ( $N_H/N > 0.14$ ) are more spherical (hence lower  $A_3$ ) and less prolate (hence lower  $S_3$ ) than their type A INNER-H counterparts. This is again due to that type B stars are more compact, even though they have certain asymmetry related to the fact that the core bead is outside the H subglobule. However, for low values of  $N_H/N$ , i.e.,  $N_H/N < 0.08$ , there is very little difference between the INNER-H and OUTER-H stars in terms of asphericity and prolateness, since the end monomers contribute little to these characteristics, in either types A or D. Generally, for both types A and B, increasing  $N_H/N$  results in more spherical shapes as the H subglobule increasingly dominates. As can be observed in Fig. 2a, the typical snapshots of type C stars are quite asymmetrical, explaining the relatively large values for both  $A_3$  and  $S_3$  in the region corresponding to type C stars.

## C. Intrachain monomer–monomer radial distribution functions

The monomer–monomer radial distribution functions (RDF),  $g_{ij}^{(2)}(r)$ , between monomers  $i$  and  $j$ , are useful in providing statistical information on the internal structure of conformations adopted by polymers<sup>42</sup>. We report here the rescaled versions of these functions, in terms of dimensionless variables after rescaling via the MS distances between monomers  $i$  and  $j$ , as discussed in Ref. 42, namely,

$$\hat{g}_{ij}^{(2)}(\hat{r}_{ij}) \equiv D_{ij}^{3/2} g_{ij}^{(2)}(r), \quad \hat{r}_{ij} \equiv \frac{r}{\sqrt{D_{ij}}}, \quad D_{ij} \equiv \langle (\mathbf{X}_i - \mathbf{X}_j)^2 \rangle. \quad (8)$$

This rescaling allows one to perform a more straightforward comparisons between different systems and sizes and highlights the universality properties of the RDF<sup>42</sup>.

Since there are large numbers of different  $\hat{g}_{ij}^{(2)}$  types, we would be only interested in discussing here the novel features present in copolymer stars. In the poor solvent, the topology of most flexible homopolymers becomes less significant, except locally<sup>41</sup>. Indeed, the H-H RDFs behave pretty much as in the homopolymer globules with an oscillating shape. Behaviour of most of the P-P RDFs are also broadly akin to those of homopolymer coils with a power law fall at small distances (‘correlation hole’) and a stretched exponential decay at large ones<sup>42</sup>, although the effect of double constraint in the loopy micelle (type B) is quite significant. Nevertheless, it would be most interesting to investigate the mixed H-P RDFs which have no homopolymer analogues. As the monomers inside the H globules are nearly equivalent to each other as we have seen above, we can further average the functions  $\hat{g}_{ij}^{(2)}$  over  $i$  values belonging to the H section, thereby improving the statistics.

From Figs. 8 and 9, we can determine how certain representative monomers in the polar block align themselves with regard to the hydrophobic globular blocks, in various different stars. We report these plots for  $N_H/N = N_P/N = 0.5$  composition. Naïvely, one could expect that the hydrophobic globule can simply be treated as a ‘core monomer’, albeit a rather large one. Hence the  $\hat{g}_{H,end}^{(2)}(\hat{r})$  functions should behave similarly to the  $\hat{g}_{ij}^{(2)}(\hat{r})$  functions between monomers in the arms and the core monomer of a homopolymer star in good solvent, as in Ref. 42. Indeed, if one neglects the interactions between hydrophobic monomers and polar monomers, this is what would result. As we have

mentioned previously in Section II, we treat the H-P interactions as being the arithmetic mean of the interactions between two monomers of the same type, using the rationale discussed in Refs. 39, 43. This model then yields a slight attraction of polar monomers for the hydrophobic monomers in the globule for the parameter values considered here. This weak very short-ranged attraction causes the polar blocks to wrap around the hydrophobic globule, resulting in the occurrence of a peak for small values of  $\hat{r}$  in  $\hat{g}_{H,end}^{(2)}(\hat{r})$  near the steric contact separation for the RDF between the end P-monomers and the H-monomers of INNER-H stars with  $f = 3, 6, 12$  arms in Fig. 8. Other small peaks (reflecting the ‘microstructure’ of the conformation) correspond to higher order preferential solvation ‘shells’ of the H-subglobule as in Fig. 5 in Ref. 42. These peaks become less significant with increasing number of arms. However, the behaviour for large values of  $\hat{r}$  is quite important as the tails of the plots with increasing numbers of arms do not overlap for large values of  $\hat{r}$  in Fig. 8. This can be explained by the increased steric repulsion near the centre of the star with larger  $f$ , making it more favourable for polar monomers to adopt positions away from the core. This is also manifested in the decreasing values of  $\hat{g}_{H,end}^{(2)}(\hat{r})$  for small  $\hat{r}$ , since increasing  $f$  promotes the ‘correlation hole’ effect leading to higher values of the power-law exponent  $\theta$  (see second block in Tab. II of Ref. 42).

It is also interesting to compare the RDFs of the INNER-H and OUTER-H cases. In Fig. 9a, we compare the  $\hat{g}_{ij}^{(2)}(\hat{r})$  plots between the hydrophobic globule and the monomer at the end of the polar block (i.e., the end monomers for INNER-H topologies and the core monomer for OUTER-H topologies), for both types of stars, with the same number of arms. The RDF  $\hat{g}_{H,end}^{(2)}(\hat{r})$  of INNER-H is more localised than  $\hat{g}_{H,core}^{(2)}(\hat{r})$  of OUTER-H stars in this rescaled representation, while we remember that the corresponding  $D_{ij}$  of OUTER-H stars is actually considerably smaller than for INNER-H. This can be easily explained according to our rationale in Ref. 42. Indeed, the large- $\hat{r}$  stretching exponent,  $\delta = 1/(1 - \nu)$ , for the INNER-H case gives a value close to 2.5 as  $\nu \simeq 3/5$  for the end-H interactions as in the homopolymer P-star. On the other hand, the highly constrained P-blocks of the OUTER-H loopy micelle have nearly quasi-ideal behaviour, and hence a more compact size, with  $\nu \simeq 1/2$  yielding  $\delta \simeq 2$  for the core-H interactions. We also see the first solvation and higher order microstructure peaks present here as well.

Fig. 9b compares the behaviour of two different monomers in the polar block of the same OUTER-H star. It can be seen that the RDF  $\hat{g}_{H,mid}^{(2)}(\hat{r})$  decreases somewhat faster with  $\hat{r}$  than  $\hat{g}_{H,core}^{(2)}(\hat{r})$  for these  $f = 12$  arms stars. This subtle effect can be also interpreted via a larger stretching exponent  $\delta$  for the middle-H correlations as the middle monomers close to the H-block do not quite reach the Gaussian behaviour due to higher stretching of respective P-segments. Again, we also see by comparing the functions  $\hat{g}_{H,core}^{(2)}(\hat{r})$  in Figs. 9 a and b that the microstructure oscillations decrease with increasing number of arms.

#### D. Static structure factors

Although the static structure factors (SSF) are somewhat less informative than the monomer-monomer radial distribution functions<sup>42</sup>, SSF can be readily obtained from light and neutron scattering techniques<sup>42,48,49</sup>. In particular with neutron scattering it is possible to obtain partial form factors, due to the fact that by hydrogen-deuterium isotope exchange the scattering contrast can be changed at will, allowing one to observe structural properties of selected parts of the star<sup>49</sup>. It is convenient to report SSF using rescaled Kratky forms as follows,

$$\hat{S}(\hat{q}) = \frac{q^2 R_g^2}{N} S(q), \quad \hat{q} = q \sqrt{R_g^2}, \quad (9)$$

since this is less sensitive to effects of varying  $N$ . The Kratky representation is convenient for providing information about the conformations adopted by polymers, as it highlights the deviation of the form factor of the polymer from that of a linear Gaussian coil for large values of  $q$ , which would reach a constant asymptote. Note that for the partial SSF the respective partial  $R_g^2$  is used for rescaling.

In Figs. 10 and 11, we report the SSFs calculated from the simulation results obtained for stars with  $f = 6$  arms, each of length  $N/f = 50$  beads, and INNER-H and OUTER-H topologies respectively. The cases where the H and P blocks are of equal length, i.e.,  $N_H/N = 0.5$ , are reported here. The relative statistical errors of these plots are smaller than the resolution can distinguish, due to the extensive averaging inherent in the function, and so are not included.

We have discussed in a previous work<sup>42</sup> the SSFs of homopolymer stars in good solvent with increasing arm numbers as well as several other systems. Freire *et al* have also calculated SSFs for several homopolymer stars in good solvent, using results from lattice Monte Carlo simulations<sup>50</sup>. As found experimentally<sup>48,49</sup>, for small  $\hat{q}$  the SSFs of most systems are similar when using the Kratky forms. Similar behaviour is observed in Figs. 10 and 11 for the universal area  $\hat{q} < 1$ . For linear polymers in poor solvent, i.e., globules, a maximum in  $\hat{S}(\hat{q})$  is typically reached shortly afterwards<sup>42</sup>.  $\hat{S}(\hat{q})$  then decreases until it reaches a value near zero, where it begins oscillating with increasing  $\hat{q}$ .

This is indicative of the dense structure of a globule.  $\hat{S}(\hat{q})$  for linear polymers in good solvent, i.e., coils, on the other hand, continues to increase for increasing  $\hat{q}$ <sup>42</sup>, indicative of the loose structure of coils. Stars in good solvent tend to be denser than linear polymers, and so they adopt an intermediate behaviour, with  $\hat{S}(\hat{q})$  initially decreasing after an initial maximum as for the dense globules, before starting to increase as for coils. This deviation from the behaviour of linear polymers in good solvent becomes more pronounced for larger numbers of arms<sup>42,50</sup>, corresponding to the more dense nature of many-arms stars. In poor solvent, the connectivity of stars is less significant, and they behave similarly to linear polymer globules. Naïvely, one could assume that diblock star copolymers, where half of the beads are in good solvent and half of the beads are in poor solvent, would have an intermediate behaviour between the two homopolymers. It should be remembered, however, that the behaviour of beads in the inner region of the star is different from the outer region of the star even for the simpler homopolymer in good solvent<sup>49</sup>. The inner region of stars tends to be more densely packed than the outer region. For this reason, as well as to distinguish between the effects of the H beads and the effects of the P beads on the structure, it is helpful to study the partial structure factors due to the two separate blocks as well as the total SSFs.

For both the INNER-H and OUTER-H cases in conformation B (See Fig. 10 and 11), the partial SSFs of the H beads are similar to those observed for homopolymer globules<sup>42</sup>, since the globular region of the micelles observed in Fig. 1 are densely packed. Therefore, the total SSFs of these systems seem to correspond to denser systems than their good solvent counterparts. Although the P beads in the INNER-H case appear to have a similar behaviour to those of homopolymer stars in the good solvent (in fact the slopes of the increase seem somewhat greater, suggesting a stiffening of the chains) as can be seen in Figs. 10, the P beads in the OUTER-H case behave as if they are denser, as illustrated in Figs. 11. The partial SSF  $\hat{S}_P$  appears to decrease slower at large values of  $\hat{q}$  suggesting smaller values of the swelling exponent (inverse fractal dimension) of the P-arms in the OUTER-H stars than the good solvent values  $\nu \simeq 3/5$ , possibly quite close to the quasi-ideal coil  $\nu \simeq 1/2$  as indicated by nearly constant asymptote. This could be explained by the more compact nature of the OUTER-H stars, due to the extra restriction on connectivity due to attachment to the core bead as previously discussed.

## V. CONCLUSIONS

In this paper, we have analysed the conformations adopted by a variety of different amphiphilic star diblock copolymers involving hydrophobic (H) and polar (P) monomers. In particular, we have studied the differences between stars where the hydrophobic blocks are attached to the core monomer of the star, INNER-H, and star where the polar blocks are attached to the core monomer, OUTER-H stars. Four different types of conformations were observed.

INNER-H stars all formed micellar-type conformations, where the hydrophobic monomers collapsed into a globule while the polar blocks adopted coil-like behaviour in the ‘shell’ surrounding the globule. OUTER-H stars, on the other hand were able to adopt three different types of conformations, depending on the relative ratio of the lengths of the two blocks in the arms, as well as the total length of the arms. Most OUTER-H stars were able to form ‘loopy micelle’ conformations, where the hydrophobic monomers collapsed into a globule as for INNER-H topologies, however, the polar blocks in these stars were more constrained, since they were joined at two ends, i.e., the hydrophobic globule and the core monomer. This extra constraint existed only in part of the phase diagram, since reducing the relative length of the hydrophobic block, resulted in an alternative type of conformation, where the hydrophobic blocks collapsed into small globules at the ends of each arm, but these small globules were unable to coalesce into the single larger globule of the loopy micellar conformations. For intermediate values of the relative length of the hydrophobic blocks, the energy when these small globules coalesced was similar to the energy where they did not coalesce, and hence a fourth type of conformation was observed with different types of clustering occurring. In this final type, the globules were able to separate and reform throughout equilibrium simulation. This is due to that the energy barriers between the free energy minima corresponding to different conformations in this regime appeared to be quite low, since relatively large specific heat capacities were observed for these systems indicating a larger energy variance.

Increasing the length of the arms reduced the effects of the constraint of the polar blocks in OUTER-H stars with loopy micellar conformations, and hence these conformations were observed for a wider range of hydrophobic:polar ratios for stars with longer arms. However, changing the number of arms did not seem to affect the range where these conformations were observed, although stars with more than twelve arms were not considered due to computational limitations.

When the OUTER-H stars were able to form loopy micellar conformations, they were more spherical and less prolate than their INNER-H counterparts. This was due to the fact that the OUTER-H conformations are more compact as the polar blocks are each constrained at two points.

For the two types of star topologies we have also analysed the radial distribution functions (RDF) for the mixed H-P monomer pairs, which exhibited a nontrivial behaviour, in some ways combining features of the RDFs of P-P



and H-H pairs of monomers, and investigated the influence of the number of arms.

Finally, we have computed the total and partial H- and P- static structure factors (SSF) of both INNER-H star micellar and OUTER-H star loopy micellar conformations, which could be directly tested against experimental data. These have showed the dense structure of the hydrophobic subglobule and nontrivial fractal dimension of the constrained polar blocks in the loopy micelle.

Obviously these single-chain simulations do not provide information about the inter-chain interactions which would permit one to investigate the issue of whether or not monomolecular micelles are the solitary structures for certain star copolymers at intermediate concentrations. However, the knowledge of single chain conformations structure allows us to make some predictions as to how much such unimolecular micellar objects would interact at higher concentrations.

According to Förster *et al*<sup>51,52</sup>, the mean aggregation number,  $Z$  (i.e., the number of molecules in a single micelle above the CMC), in diblock polymeric micelles (as well as low molecular weight surfactant micelles) can be determined from the empirically determined relation:  $Z = Z_0 N_A^2 N_B^{-0.8}$ , where  $Z_0$  is a parameter which depends on the polymers or surfactants used, and  $N_A$  and  $N_B$  are the degrees of polymerisation of the insoluble (H in this case) and the soluble (P in this case) blocks, respectively. They found that the aggregation number of triblock BAB (or PHP) copolymers could be determined by treating the triblock as being ‘cut’ into two diblock halves. In this way the aggregation number of the triblock is half of that for each of the two diblock halves. They generalised this model to predict the micellisation behaviour of graft copolymers, where a polymer with  $n$  grafts is cut into  $n$  pieces, each piece containing one graft. If a constant graft density,  $n/N_A$ , was assumed, the aggregation number was then predicted to decrease as  $n^{-1.51}$ . Note, however, that a similar argument is not valid for the ABA (or HPH) triblocks with hydrophobic ends (end-stickers), which are known to form extended networks and telechelic gels.

One could also apply this principle to star diblocks, hence expecting that the aggregation number will decrease as  $f^{-1}$ . If this aggregation number equals 1, then this would correspond to a ‘unimolecular micelle’. It can be seen that increasing the length of the P block decreases this number, while increasing the length of the H block increases this number as in Förster’s Eq. By increasing the length of the H block, the surface area of ‘exposed’ H monomers is increased, promoting aggregation. Increasing the length of the P block, on the other hand, allows the polar monomers to shield the hydrophobic monomers from the solvent, reducing the aggregation number as the P shell is repulsive. Intuitively, one could say that this shielding is enhanced in the OUTER-H case, since the polar blocks are ‘wrapped’ around the hydrophobic core better. With all this in mind, one could suggest that OUTER-H stars with many arms, long P blocks and short H blocks are most likely to form only unimolecular micelles. Obviously the choice of monomers is also important, as this affects  $Z_0$ . In the INNER-H case larger number of arms  $f$  would be required to form a sufficiently prohibitive polar shell to suppress further aggregation. We hope to be able to investigate these questions directly via multi-star simulations in the future.

## ACKNOWLEDGMENTS

We are grateful to Professor Giuseppe Allegra, Professor Fabio Ganazzoli, Dr Guido Raos, Giovanni Bellesia and Stefano Elli for interesting discussions. We would also like to thank Adam Byrne for his efforts during the course of his undergraduate project.

- 
- <sup>1</sup> G. S. Grest, L. J. Fetters, J. S. Huang, *Adv. Chem. Phys.*, **94**, 67 (1996).  
<sup>2</sup> K. Ishizu, S. Uchida, *Prog. Polym. Sci.*, **24**, 1439 (1999).  
<sup>3</sup> J. Roovers, L.-L. Zhou, P. M. Toporowski, M. van der Zwan, H. Iatrou, N. Hadjichristidis, *Macromolecules*, **26**, 4324 (1993).  
<sup>4</sup> A. Heise, J. L. Hedrick, M. Trollsås, R. D. Miller, C. W. Frank, **32**, 231 (1999).  
<sup>5</sup> J. L. Hedrick, M. Trollsås, C. J. Hawker, B. Atthof, H. Claesson, A. Heise, R. D. Miller, D. Mecerreyes, R. Jérôme, Ph. Dubois, *Macromolecules*, **31**, 8691 (1998).  
<sup>6</sup> N. Hadjichristidis, S. Pispas, M. Pitsikalis, H. Iatrou, C. Vlahos, *Adv. Polym. Sci.*, **142**, 72 (1999).  
<sup>7</sup> S. Kanaoka, S. Nakata, H. Yamaoka, *Macromolecules*, **35**, 4564 (2002).  
<sup>8</sup> Y. C. Bae, R. Faust, *Macromolecules*, **31**, 2480 (1998).  
<sup>9</sup> C. Tsitsilianis, D. Papanagopoulos, P. Lutz, *Polymer*, **36**, 3745 (1995).  
<sup>10</sup> J. Feldthusen, B. Iván, A. H. E. Müller, *Macromolecules*, **31**, 578 (1998).  
<sup>11</sup> C.-M. Dong, K.-Y. Qiu, Zh.-W. Gu, X.-D. Feng, *Macromolecules*, **34**, 4691 (2001).  
<sup>12</sup> S. Uchida, A. Ichimura, K. Ishizu, *Polymer*, **40**, 1019 (1999).

- <sup>13</sup> P. Kurian, S. Zschoche, J. P. Kennedy, *J. Polym. Sci. A: Polym. Chem.*, **38**, 3200 (2000).
- <sup>14</sup> P. Cai-Yuan, T. Lei, Wu De-Cheng, *J. Polym. Sci. A: Polym. Chem.*, **39**, 3062 (2001).
- <sup>15</sup> R. S. Saunders, R. E. Cohen, S. J. Wong, R. R. Schrock, *Macromolecules*, **25**, 2055 (1992).
- <sup>16</sup> Y. K. Choi, Y. H. Bae, S. W. Kim, *Macromolecules*, **31**, 8766 (1998).
- <sup>17</sup> Y. Li, T. Kissel, *Polymer*, **39**, 4421 (1998).
- <sup>18</sup> S. Kanaoka, M. Sawamoto, T. Higashimura, *Macromolecules*, **24**, 5741 (1991).
- <sup>19</sup> S. Angot, D. Taton, Y. Gnanou, *Macromolecules*, **33**, 5418 (2000).
- <sup>20</sup> A. Heise, J. L. Hedrick, C. W. Frank, R. D. Miller, *J. Am. Chem. Soc.*, **121**, 8647 (1999).
- <sup>21</sup> B. S. Lele, J.-C. Leroux, *Polymer*, **43**, 5595 (2002).
- <sup>22</sup> X. Chen, J. Smid, *Langmuir*, **12** 2207 (1996).
- <sup>23</sup> Y.-I. Jeong, J.-W. Nah, H.-C. Lee, S.-H. Kim, C.-S. Cho, *Int. J. Pharm.*, **188**, 49 (1999).
- <sup>24</sup> D. Taton, E. Cloutet, Y. Gnanou, *Macromol. Chem. Phys.*, **199**, 2501 (1998).
- <sup>25</sup> B. Jeong, Y. K. Choi, Y. H. Bae, G. Zentner, S. W. Kim, *J. Controlled Release*, **62**, 109 (1999).
- <sup>26</sup> H. Liu, S. Farrell, K. Urich, *J. Controlled Release*, **68**, 167 (2000).
- <sup>27</sup> C. Allen, D. Maysinger, A. Eisenberg, *Colloids Surf., B*, **16**, 3 (1999).
- <sup>28</sup> T. Inoue, G. Chen, K. Nakamae, A. S. Hoffman, *J. Controlled Release*, **51**, 221 (1998).
- <sup>29</sup> A. Lavasanifar, J. Samuel, G. S. Kwon, *Adv. Drug Deliv. Rev.*, **54**, 169 (2002).
- <sup>30</sup> S. Y. Kim, I. G. Shin, Y. M. Lee, C. S. Cho, Y. K. Sung, *J. Controlled Release*, **51**, 13 (1998).
- <sup>31</sup> J.-G. Ryu, Y.-I. Jeong, Y.-H. Kim, I.-S. Kim, D.-H. Kim, S.-H. Kim, *Bull. Korean Chem. Soc.*, **22**, 467 (2001).
- <sup>32</sup> H. Liu, A. Jiang, J. Guo, K. E. Urich, *J. Polym. Sci. A: Polym. Chem.*, **37** 703 (1999).
- <sup>33</sup> M. Gauthier, L. Tichagwa, J. S. Downey, S. Gao, *Macromolecules*, **29**, 519 (1996).
- <sup>34</sup> G. R. Newkome, C. N. Moorefield, G. R. Baker, M. J. Saunders, S. H. Grossman, *Angew. Chem. Int. Ed. Engl.*, **30**, 1178 (1991).
- <sup>35</sup> S. Stevelmans, J. C. M. van Hest, J. F. G. A. Jansen, D. A. F. J. van Boxel, E. M. M. de Brabander-van den Berg, E. W. Meijer, *J. Am. Chem. Soc.*, **118**, 7398 (1996).
- <sup>36</sup> A. Kikuchi, T. Nose, *Polymer*, **37**, 5889 (1996).
- <sup>37</sup> A. Kikuchi, T. Nose, *Macromolecules*, **29**, 6770 (1996).
- <sup>38</sup> I. Gitsov, J. M. J. Fréchet, *J. Am. Chem. Soc.*, **118**, 3785 (1996).
- <sup>39</sup> F. Ganazzoli, Yu. A. Kuznetsov, E. G. Timoshenko, *Macromol. Theory Simul.*, **10**, 325 (2001).
- <sup>40</sup> P. H. Nelson, G. C. Rutledge, T. A. Hatton, *Comput. Theor. Polym. Sci.*, **8**, 31 (1998).
- <sup>41</sup> E. G. Timoshenko, Yu. A. Kuznetsov, R. Connolly, *J. Chem. Phys.*, **117**, 9050 (2002).
- <sup>42</sup> E. G. Timoshenko, Yu. A. Kuznetsov, R. Connolly, *J. Chem. Phys.*, **116**, 3905 (2002).
- <sup>43</sup> E. G. Timoshenko, Yu. A. Kuznetsov, *J. Chem. Phys.*, **112**, 8163 (2000).
- <sup>44</sup> N. Metropolis, A. W. Rosenbluth, M. N. Rosenbluth, A. H. Teller, E. Teller, *J. Chem. Phys.*, **21**, 1087 (1953).
- <sup>45</sup> M. P. Allen, D. J. Tildesley, 'Computer Simulations of Liquids', (Clarendon Press, Oxford, 1987).
- <sup>46</sup> Note that for the heat capacity, the following formula should be used instead for the error:  

$$\pm(N(k_B T)^2 \sqrt{Q})^{-1} \sqrt{\langle(\Delta E)^4\rangle - \langle(\Delta E)^2\rangle^2}.$$
- <sup>47</sup> A. Forni, F. Ganazzoli, M. Vacatello, *Macromolecules*, **30**, 4737 (1997).
- <sup>48</sup> D. Richter, B. Stühn, B. Ewen, D. Nерger, *Phys. Rev. Lett.*, **58**, 2462 (1987).
- <sup>49</sup> D. Richter, B. Farago, L. J. Fetters, J. S. Huang, B. Ewen, *Macromolecules*, **23**, 1845 (1990).
- <sup>50</sup> L. A. Molina, A. Rey, J. J. Freire, *Comput. Theor. Polym. Sci.*, **7**, 243 (1997).
- <sup>51</sup> S. Förster, M. Zisenis, E. Wenz, M. Antonietti, *J. Chem. Phys.*, **104**, 9956 (1996).
- <sup>52</sup> S. Förster, M. Antonietti, *Adv. Mater.*, **10**, 195 (1998).

FIG. 1. A phase diagram of star copolymers with a fixed number of arms  $f$  obtained from the data for stars of  $f = 3, 6, 9, 12$  arms with illustrations of their conformations in terms of the composition,  $N_P/N$ , and the arm length,  $N/f$ . Both INNER-H and OUTER-H stars are represented on the same diagram by showing the composition of INNER-H stars with  $(N_P/N) - 1$ . Thus, the leftmost (rightmost) points on both parts correspond to totally H (P) homopolymer stars. Distinct possible conformations are designated by the letters A, B, C and D. Typical snapshots for A and B are also incorporated into the figure (these are shown for stars with  $f=12$  arms of 100 monomers each). Snapshots for C and D are shown in Fig. 2. Here and below the light gray spheres represent polar (P) monomers, while the black spheres represent hydrophobic (H) monomers.

FIG. 2. Typical snapshots of conformations of an OUTER-H  $f=12$  arm star with each arm 100 monomers long. Fig. a is that of a star with  $N_P/N = 0.92$  and Fig. b is of a star with  $N_P/N = 0.95$ . Fig. a corresponds to a star with conformation of type C and Fig. b corresponds to a star with conformation D. It can be seen that the H monomers at the end of each arm are able to cluster together to form subglobules. In Fig. a, type C conformation, some of these globular ends are further able to cluster together, in this case forming three clusters. The number of such clusters ranged from three to five during the course of the simulation.

FIG. 3. The dimensionless specific heat capacity,  $c_V/k_B$ , of INNER-H and OUTER-H stars with  $f = 6$  arms of  $N/f = 50$  monomers long vs the hydrophobic composition,  $N_H/N$ .

FIG. 4. The mean-squared radii of gyration,  $\langle R_g^2 \rangle$ , (in units of the bond length  $\ell$ ) of INNER-H and OUTER-H star copolymers with  $f = 6$  arms of  $N/f = 50$  monomers long vs the hydrophobic composition,  $N_H/N$ .

FIG. 5. The mean-squared distances of the beads from the centre-of-mass,  $\langle R_i^2 \rangle$ , (in units of the bond length  $\ell$ ) vs the chain index  $i/(N/f)$  along an arm for OUTER-H stars with  $f = 6$  and  $N/f = 50$  with different composition ratios. Curves correspond (from bottom to top) to:  $N_P/N = 0.10, 0.30, 0.50, 0.70, 0.80, 0.82, 0.84, 0.86, 0.88, 0.90, 0.92, 0.94, 0.96, 0.98$  and  $1.00$ .

FIG. 6. The asphericity index,  $A_3$ , vs the hydrophobic composition,  $N_H/N$ , for INNER-H and OUTER-H stars of  $f = 6$  arms  $N/f = 50$  monomers long.

FIG. 7. The ellipsoid index,  $S_3$ , vs the hydrophobic composition,  $N_H/N$ , for INNER-H and OUTER-H stars of  $f = 6$  arms  $N/f = 50$  monomers long.

FIG. 8. Plots of the rescaled dimensionless monomer-monomer radial distribution functions between the H monomers and the end P monomers,  $\hat{g}_{H,end}^{(2)}(\hat{r})$  vs the rescaled dimensionless radius,  $\hat{r}$  for INNER-H stars with  $f = 3, 6, 12$  arms  $N/f = 50$  monomers long and,  $N_H/N = 0.5$  composition.

FIG. 9. Plots of rescaled monomer-monomer radial distribution functions,  $\hat{g}_{ij}^{(2)}(\hat{r})$  vs the rescaled radius,  $\hat{r}$  for copolymers stars with  $N/f = 50$ . Fig. a contains the function between the end monomers and the H monomers of an INNER-H star (solid line) as well as the function between the core monomer and the H monomers of an OUTER-H star (long-dashed line), both of  $f=6$  arms with  $N_H/N=0.5$  composition. The inset (Fig. b) contains the function between the core monomer and the H monomers of an OUTER-H star (long-dashed line) as well as the function between the hydrophobic monomers and the middle monomers of the P-block (short-dashed curve) for stars with  $f = 12$  arms of  $N/f = 50$  monomers long and  $N_H/N=0.5$  composition.

FIG. 10. Kratky plots of the rescaled dimensionless static structure factor  $\hat{S}$  vs the rescaled dimensionless wave number  $\hat{q}$  for an INNER-H star with  $f = 6$  arms  $N/f = 50$  monomers long and  $N_H/N = 0.5$  composition. Here and below the solid line corresponds to the total SSF of both H and P beads, the long-dashed curve to the partial SSF of the H beads, and the short-dashed curve to the partial SSF of the P beads. Note that the partial MS radii of gyration have been used to rescale the partial SSF.

FIG. 11. Kratky plots of the rescaled static structure factor  $\hat{S}$  vs the rescaled wave number  $\hat{q}$  for an OUTER-H star in conformation type B with  $f = 6$  arms  $N/f = 50$  monomers long and  $N_H/N = 0.5$  composition.

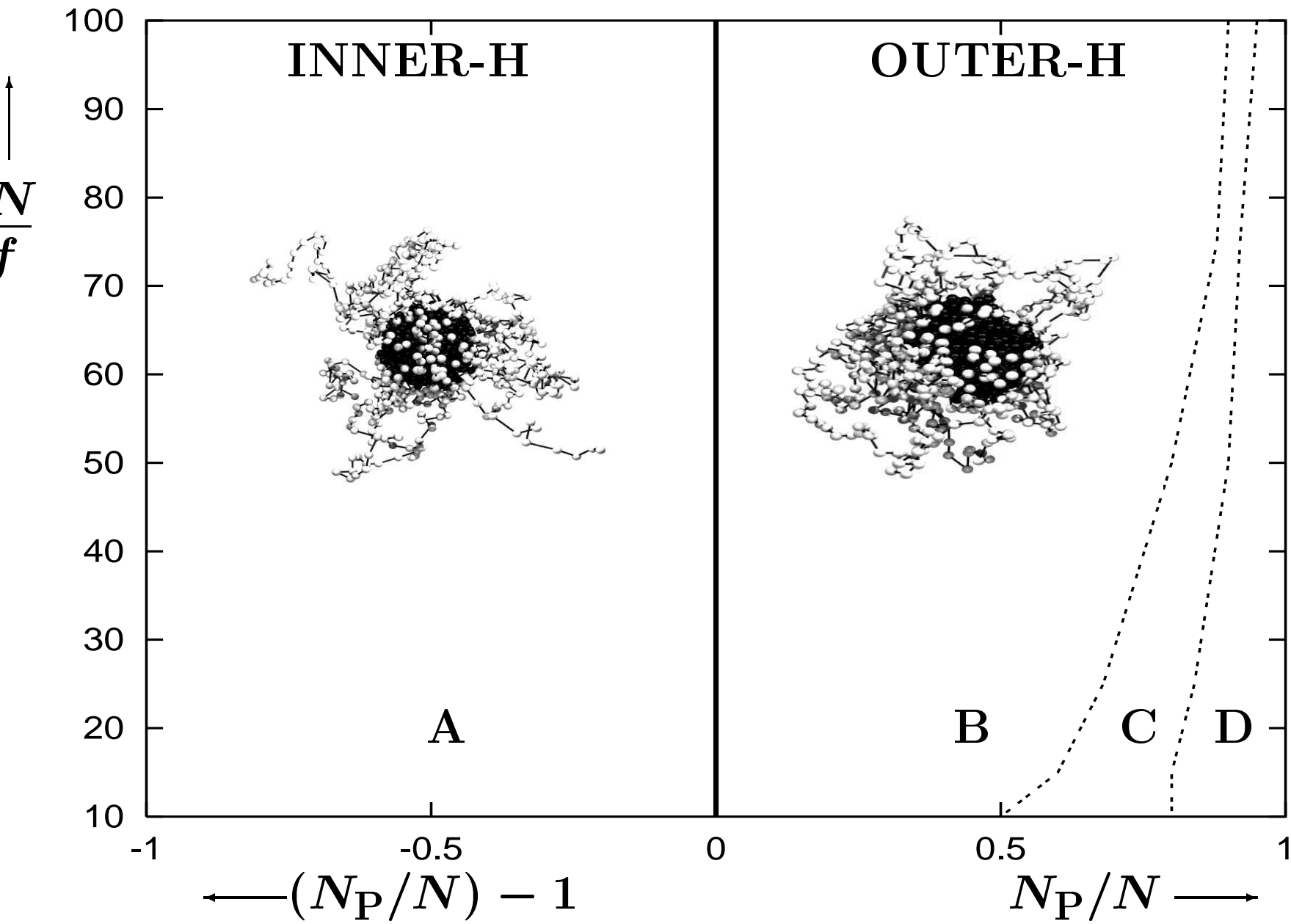


Fig. 1

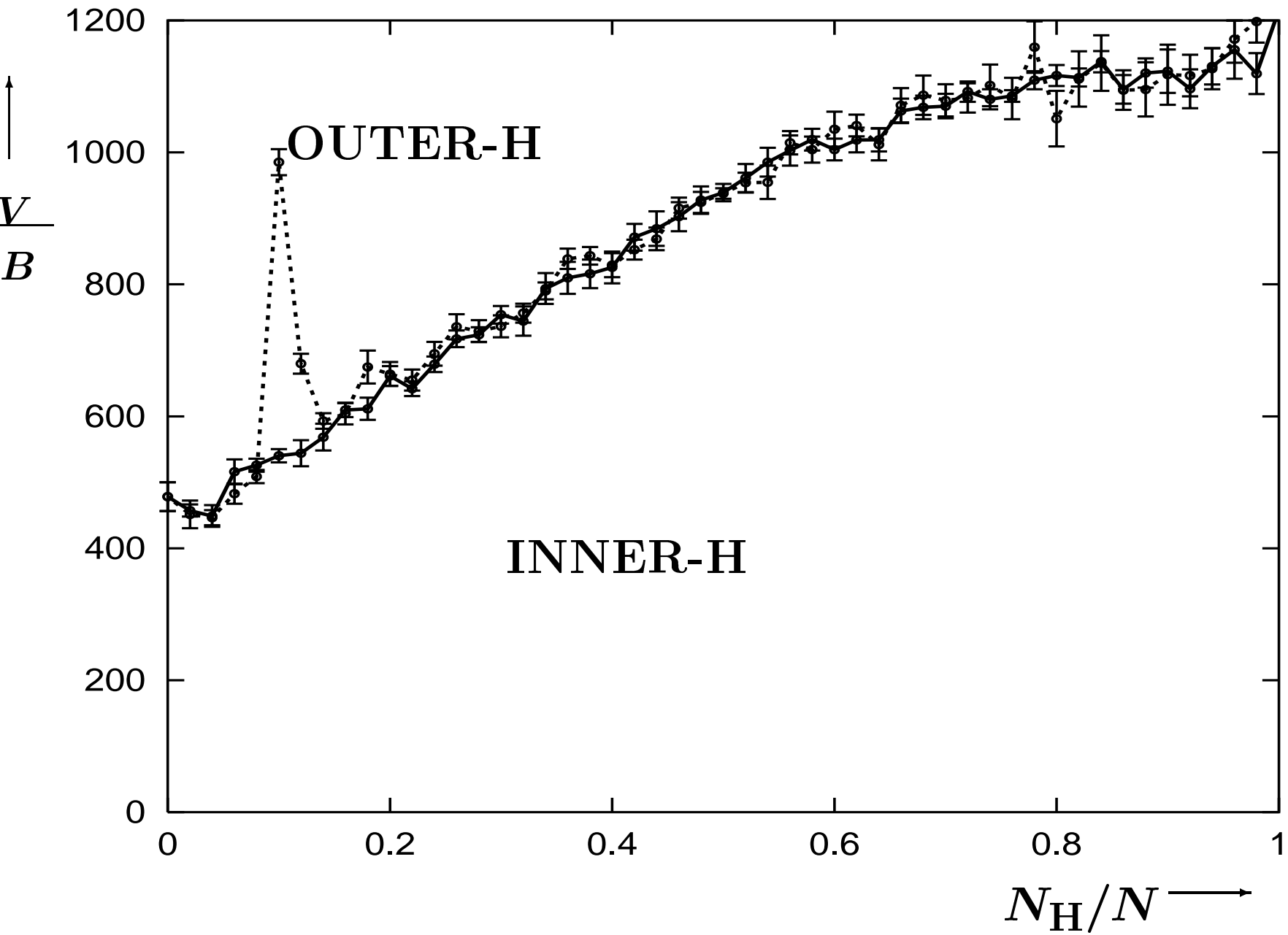


Fig. 3

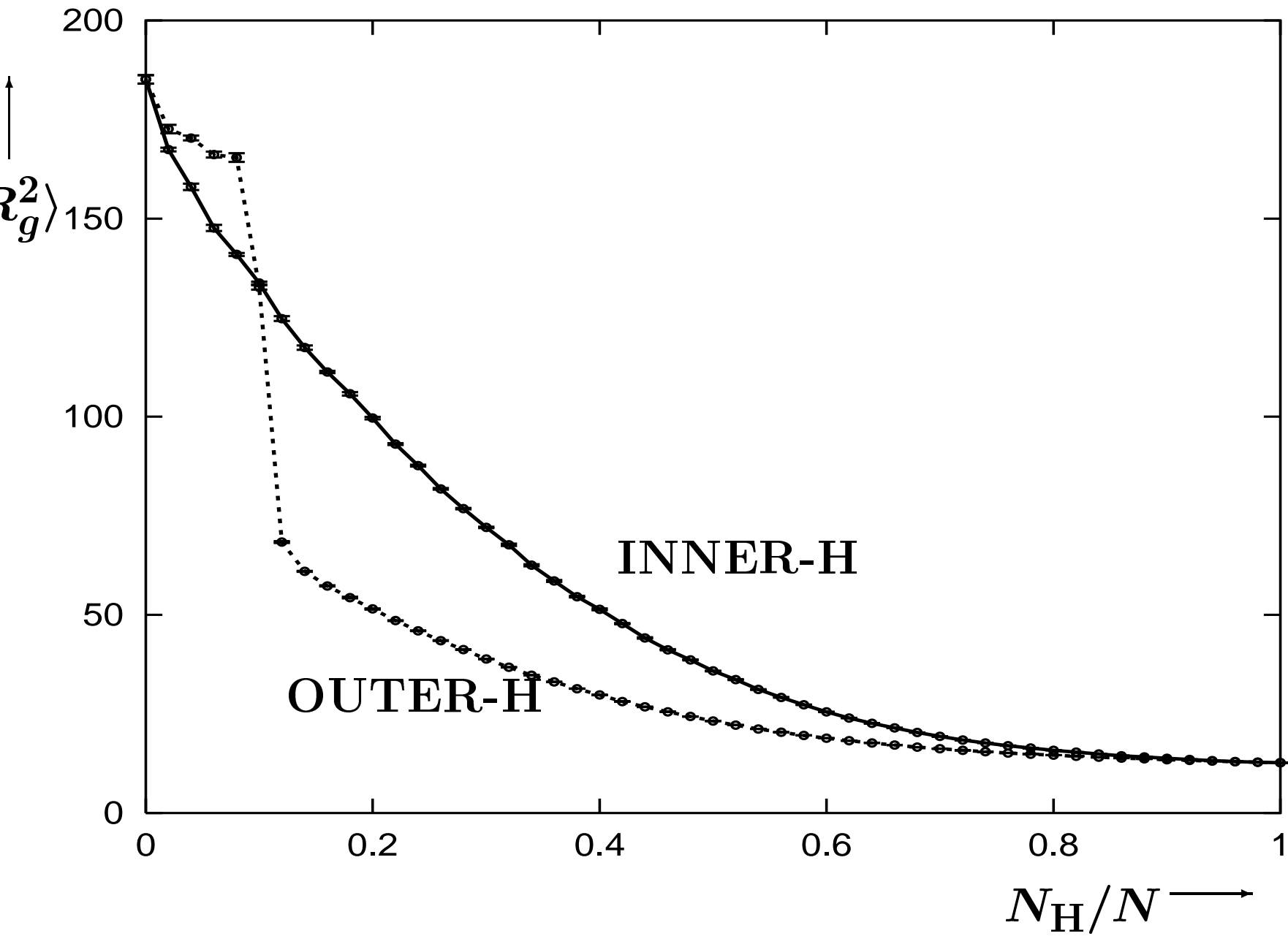


Fig. 4

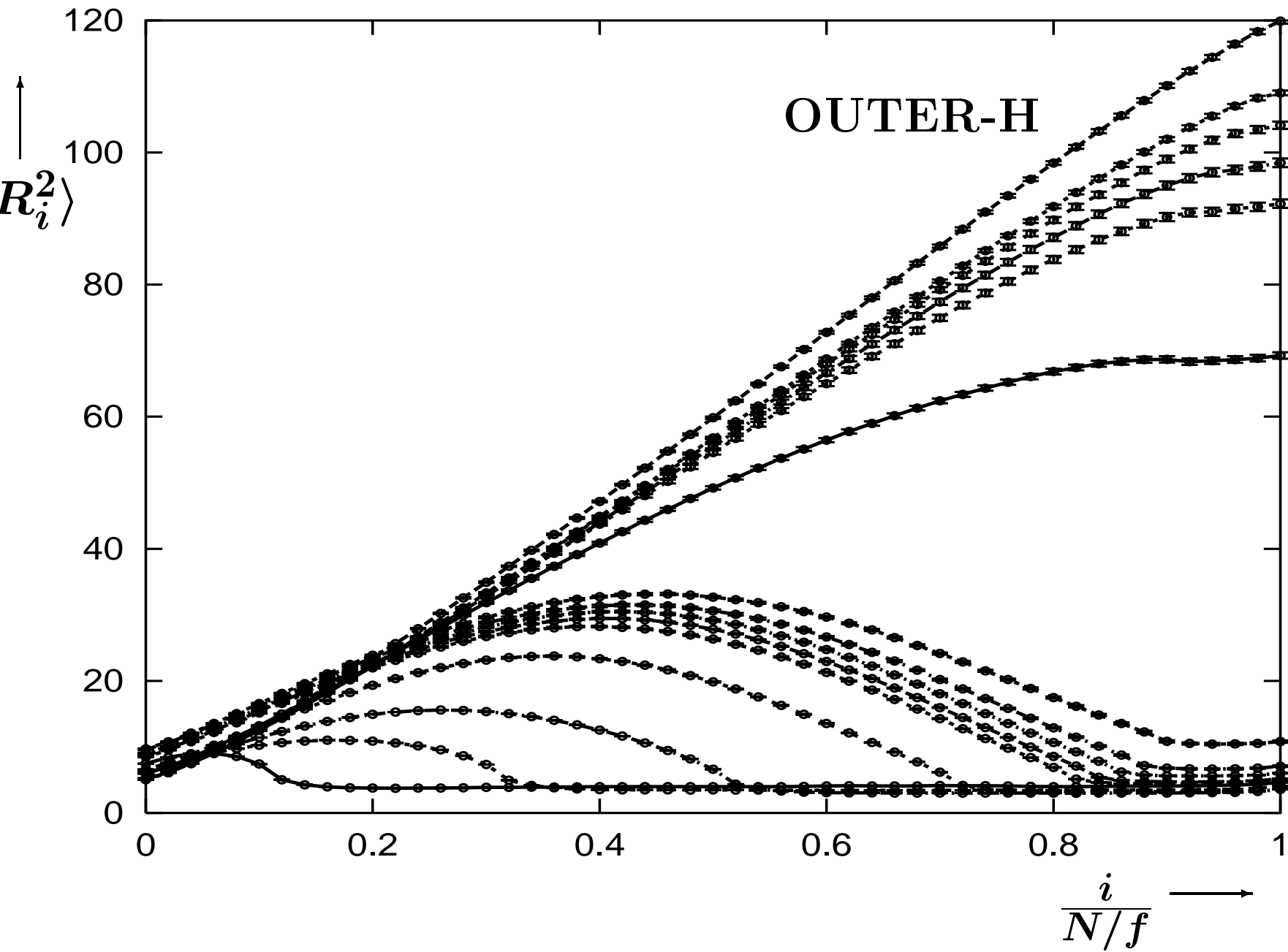


Fig. 5



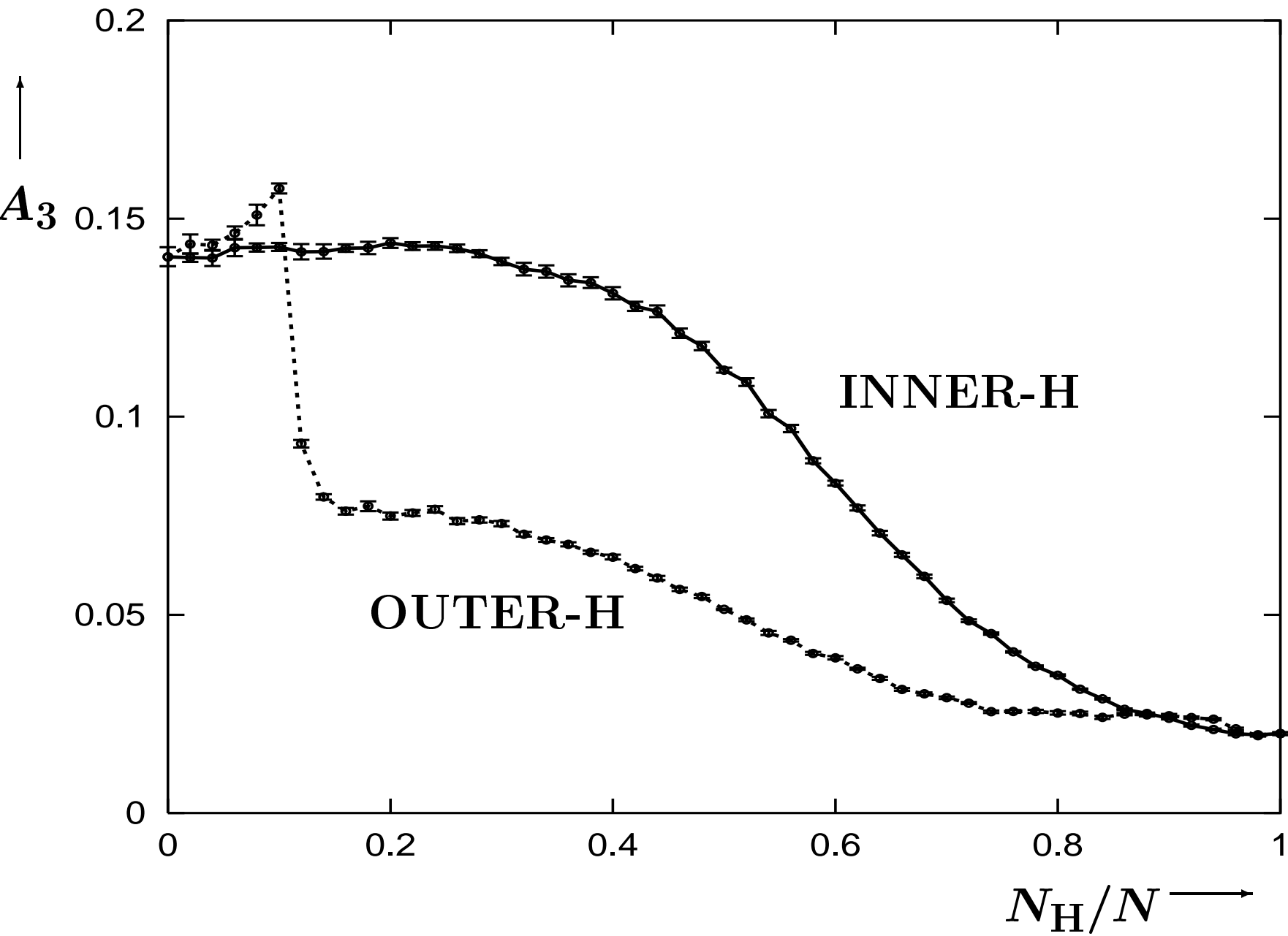


Fig. 6

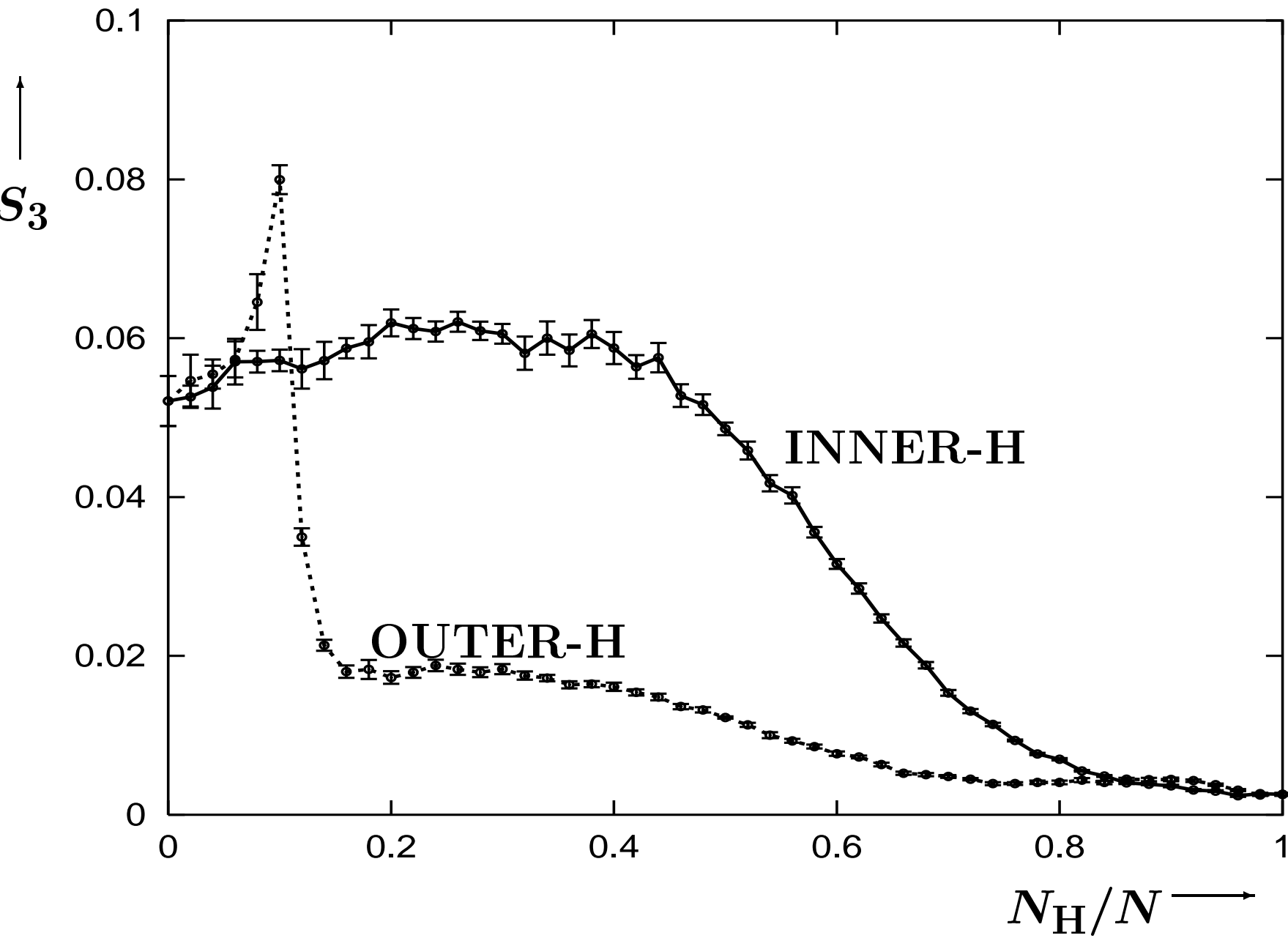


Fig. 7

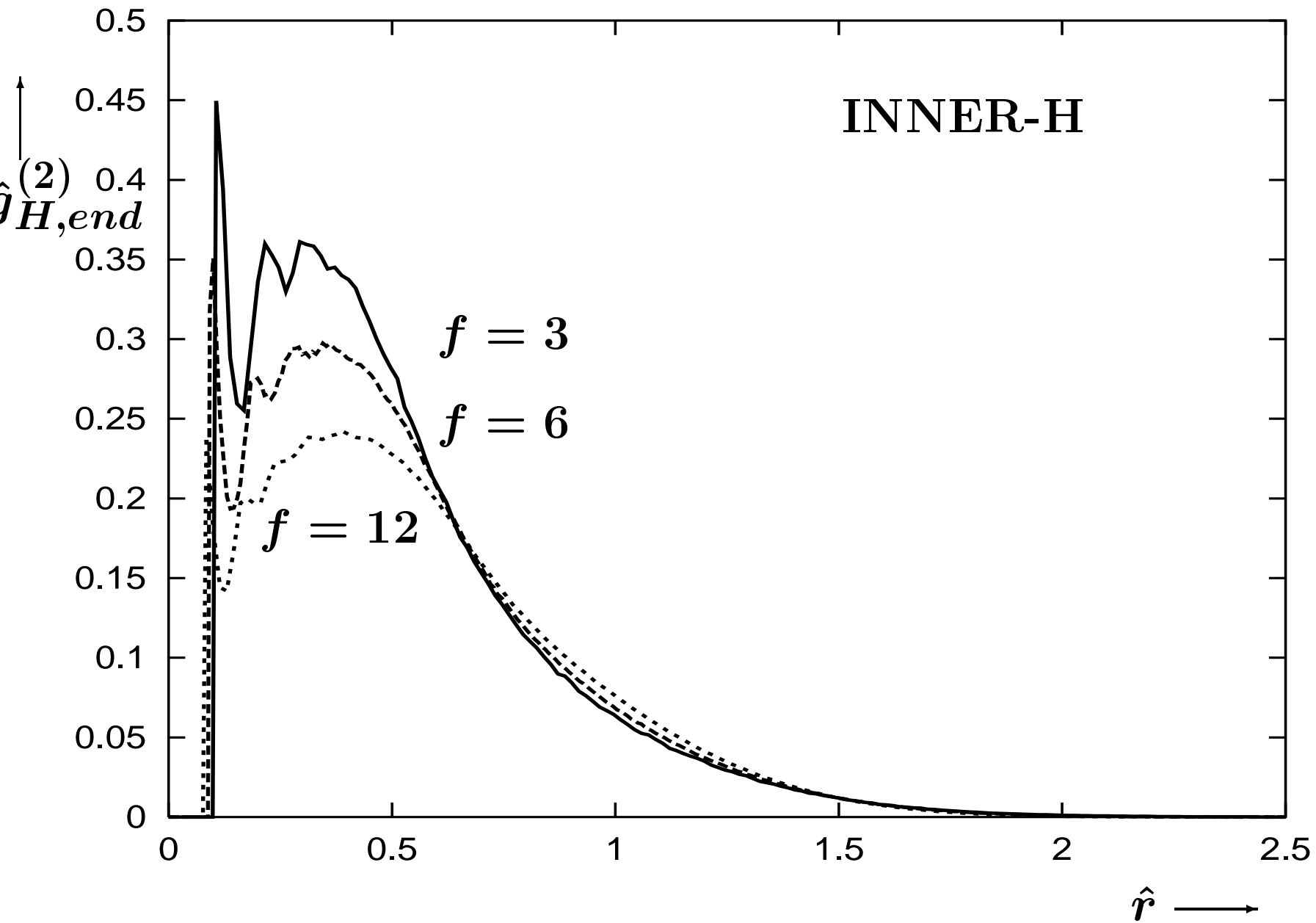


Fig. 8

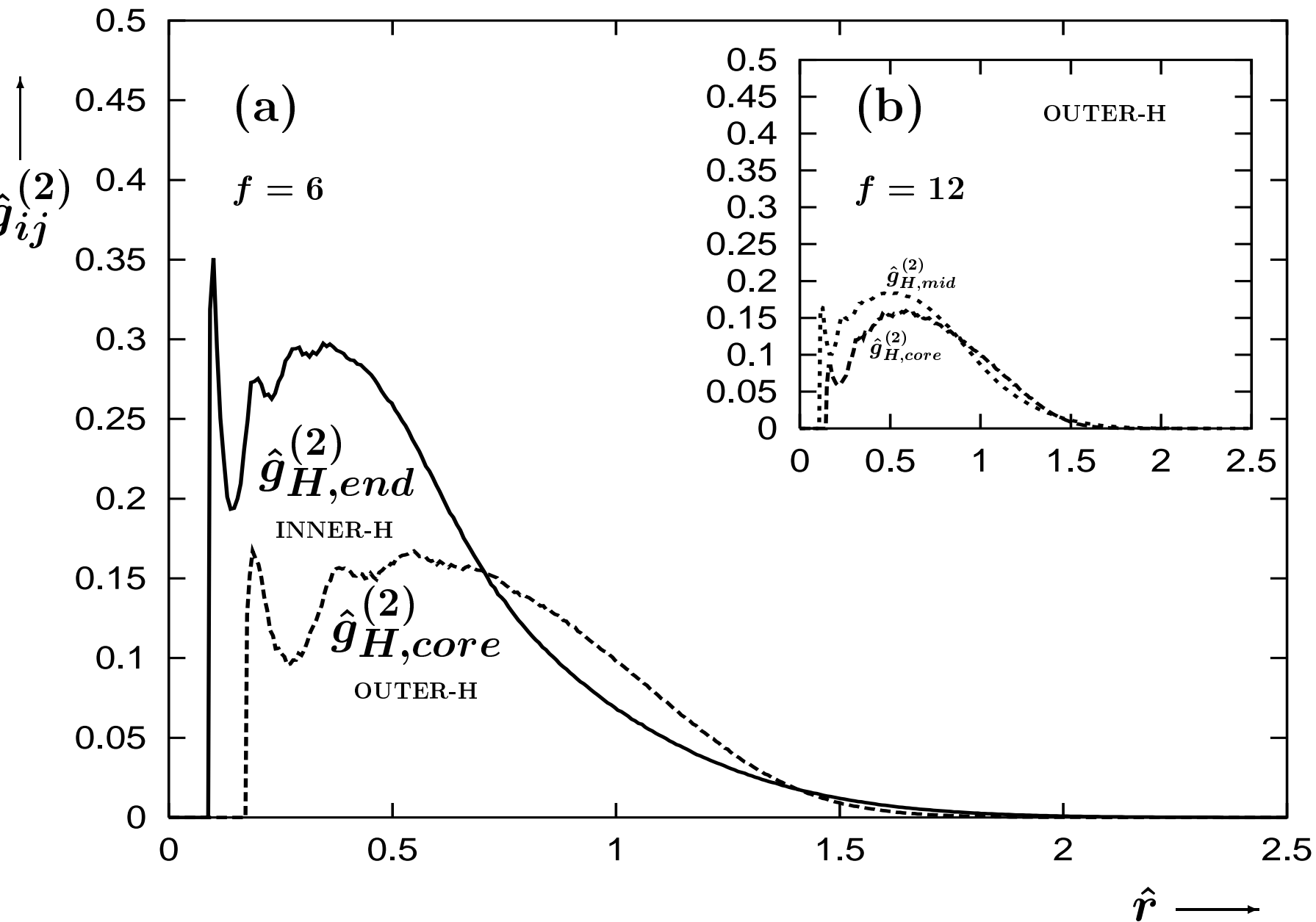


Fig. 9

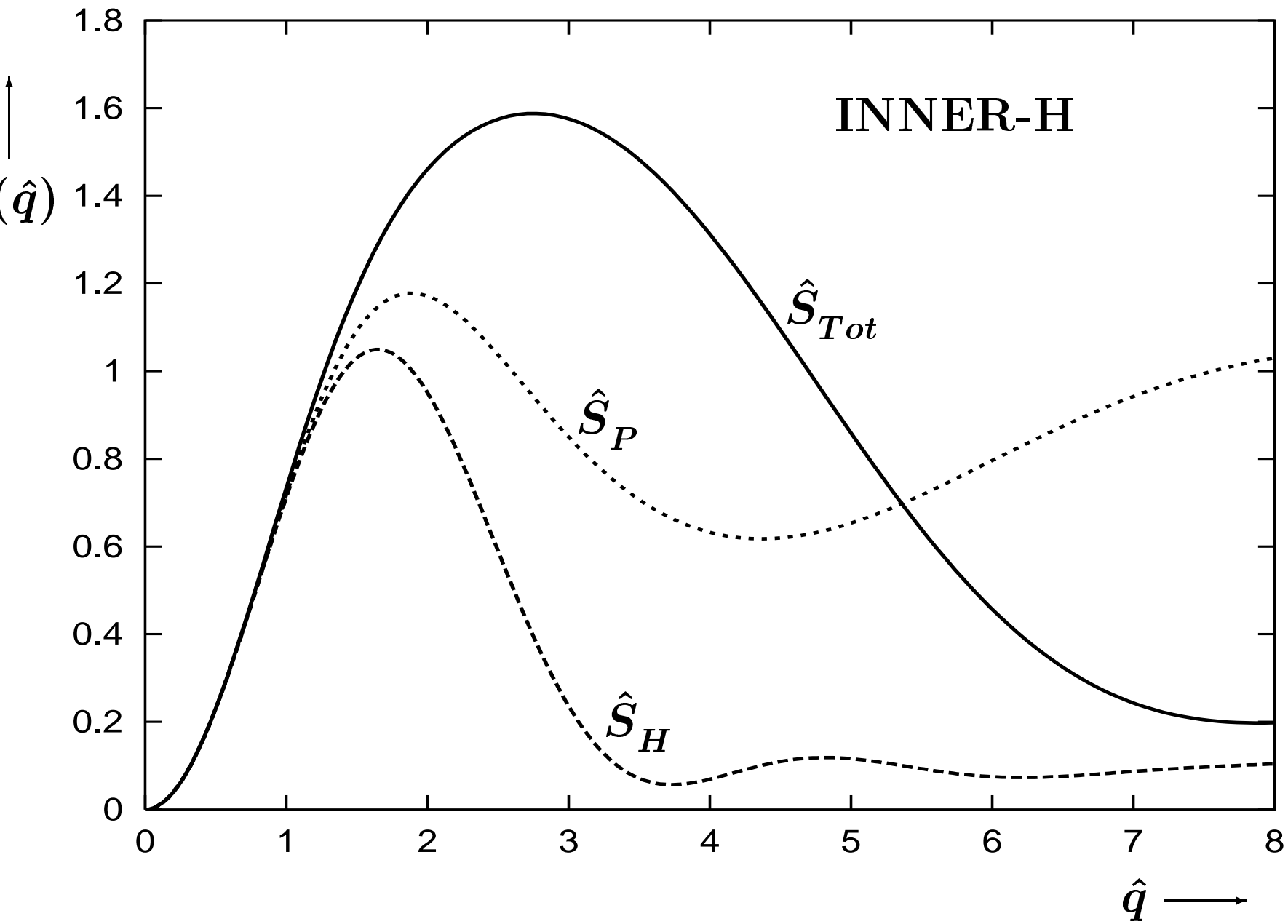


Fig. 10

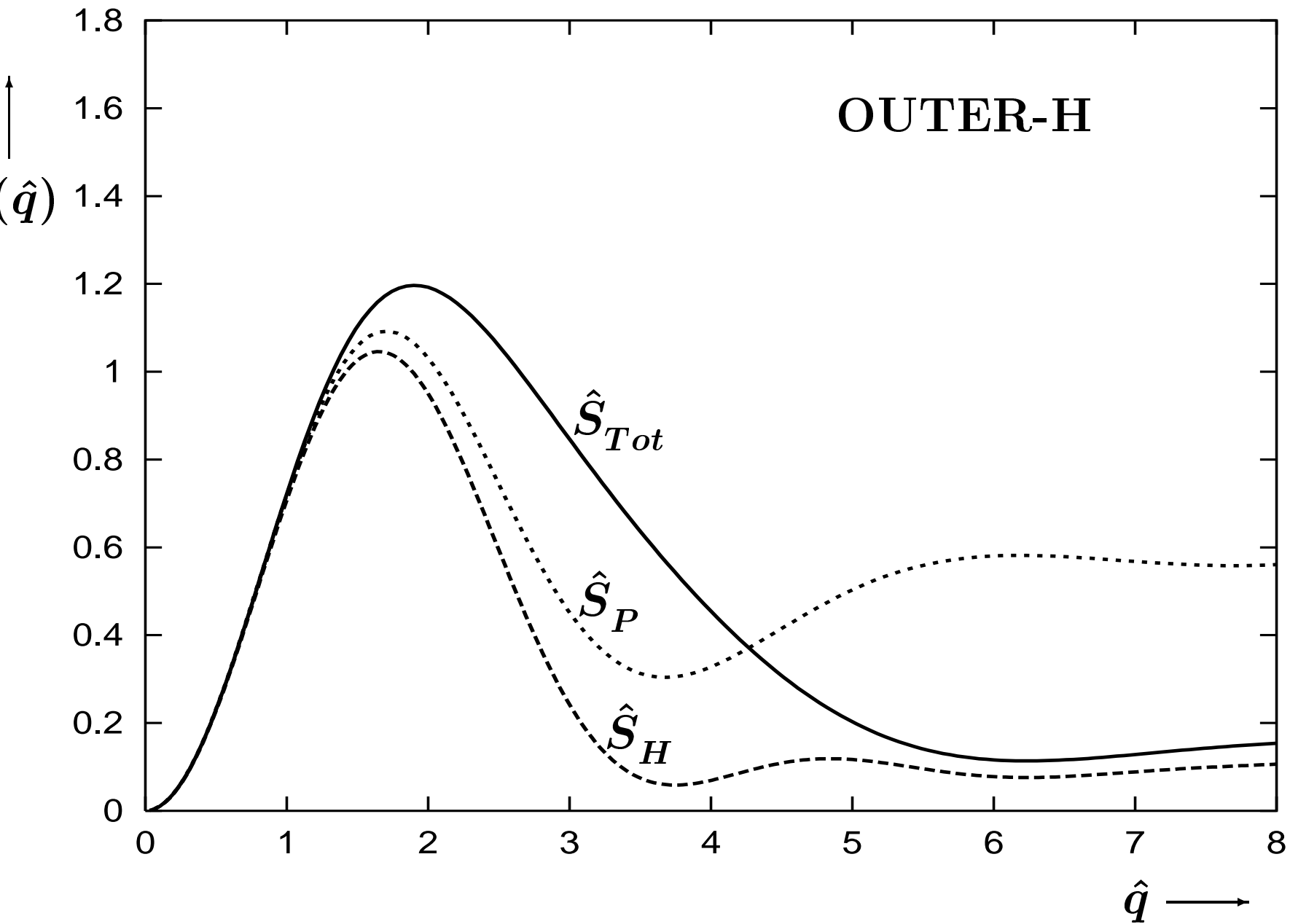
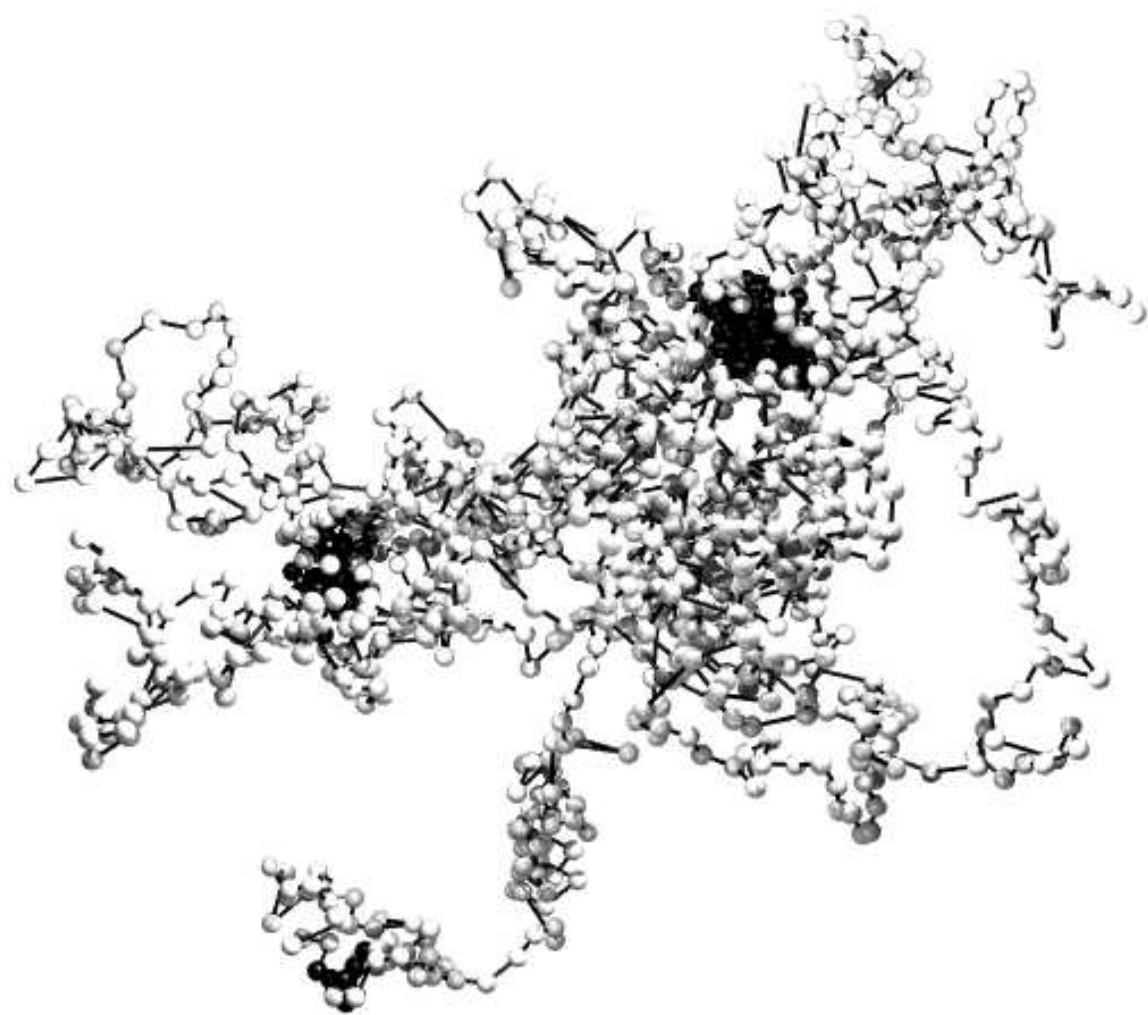
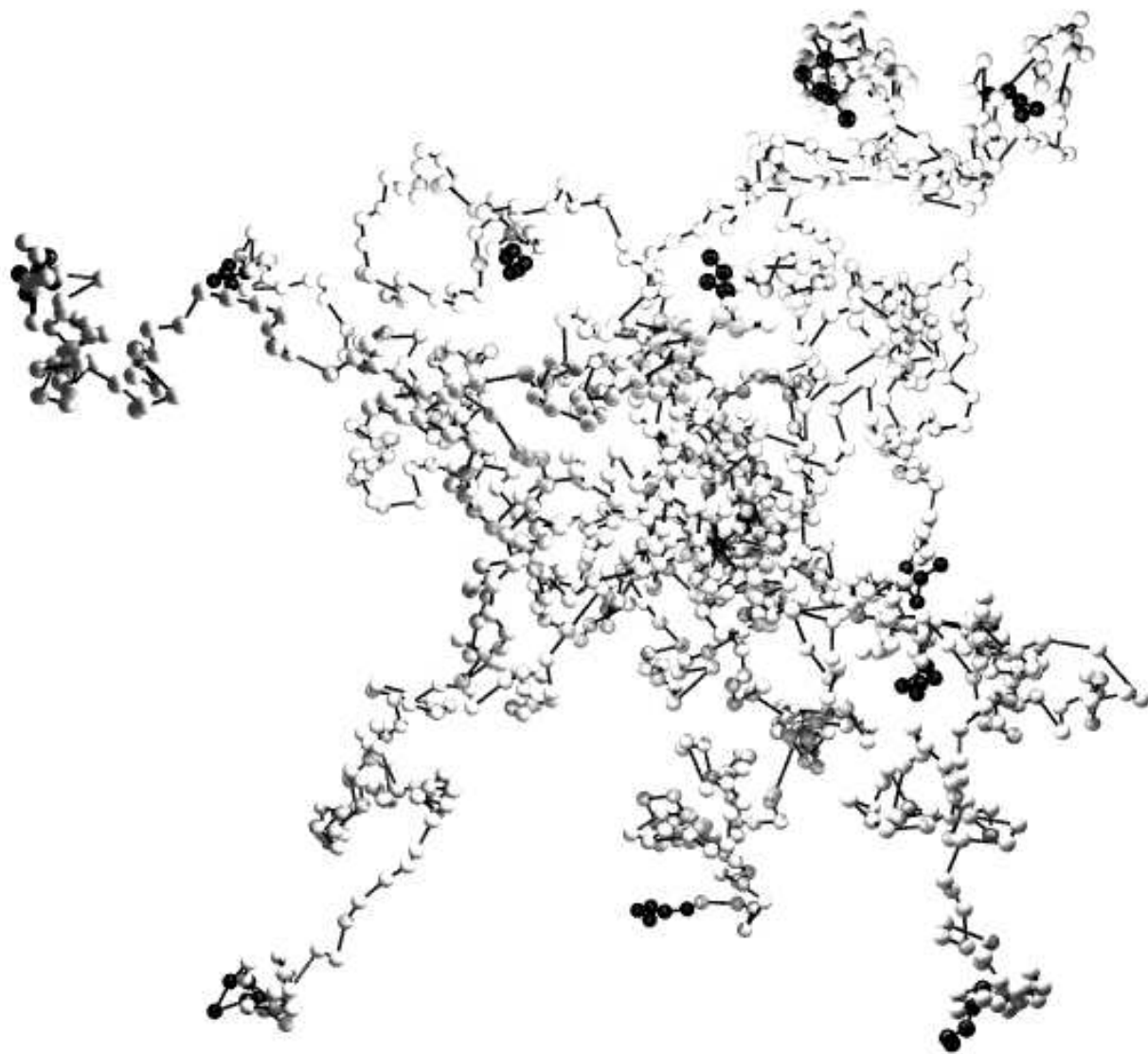


Fig. 11



**Fig. 2a**



**Fig. 2b**